Pressure-induced evaporation dynamics of gold nanoparticles on oxide substrate

Gang Meng,[1] Takeshi Yanagida,[1,*] Masaki Kanai,[1] Masaru Suzuki,[2] Kazuki Nagashima,[1] Bo Xu,[1] Fuwei Zhuge,[1] Annop Klamchuen,[1] Yong He,[1] Sakon Rahong,[1] Shoichi Kai,[2] and Tomoji Kawai[1,*]

[1]*The Institute of Scientific and Industrial Research, Osaka University, 8-1 Mihogaoka Ibaraki, Osaka, 567-0047, Japan*

[2]*Department of Applied Quantum Physics and Nuclear Engineering, Faculty of Engineering, Kyushu University, 744 Motooka, Nishi-ku, Fukuoka 819-0395, Japan*

(Received 11 November 2012; published 23 January 2013)

Here we report thermal evaporation dynamics of Au nanoparticles on single crystal oxide substrates, including MgO, $SrTiO_3$, and Al_2O_3. The size reduction rate of Au nanoparticles via thermal treatments is strongly dependent on not only temperature but also pressure. Lowering the pressure of inert Ar gas from 10^5 to 10 Pa increases the size reduction rate over 30 times in the temperature range 800 °C–950 °C. The temperature dependence is solely due to the variation of saturated vapor pressure of Au, whereas the pressure dependence of the surrounding inert gas can be interpreted in terms of a pressure dependence on a gas-phase diffusion of evaporated Au atoms into the surroundings. We present a simplified model to explain an evaporation dynamics, which well describes the pressure dependence on a size reduction rate of Au nanoparticles. By utilizing this useful pressure-induced evaporation dynamics, we succeeded in manipulating a size reduction of Au nanoparticle arrays down to − 10 nm diameter range from − 300 nm initial size by programming sequentially a surrounding pressure.

DOI: 10.1103/PhysRevE.87.012405 PACS number(s): 68.03.Fg, 68.35.Fx, 68.08.Bc

I. INTRODUCTION

Noble metal nanoparticles (size: 10–10^2 nm) on oxide surfaces have attracted much attention due to their various fascinating characteristics, including catalytic, optical, and electronic properties for energy conversion; environmental applications [1–3]; and also as seeds for nanostructure formation [4–27]. For example, Au nanoparticles on oxides exhibit a distinct catalytic property, which has not been observable in bulk Au [28]. Defining and tuning a size range of metal nanoparticles on oxide surfaces is essential to manipulating such size-dependent properties [29,30]. In addition, monodisperse nanoparticle arrays on oxide substrates offer an interesting tool to study the size dependence on their properties in the absence of size distributions [31]. Existing conventional lithographic technologies, including electron beam lithography, photolithography, and imprinting lithography, allow us to fabricate such nanoparticle arrays down to a scale of several tens of nanometers [32,33]. However, it is still rather challenging to form nanoparticle arrays on insulative oxide substrates in the size range below 50 nm, especially for a large scale [34,35]. Thermal evaporation is the simplest way to reduce the size of subjects via a mass transport through an interface [36,37]. Although this facile evaporation technique is clearly capable of reducing the meansize of nanoparticles on oxide surfaces, a knowledge of the feasibility and the detailed mechanisms as to an evaporation dynamics of metals on oxide surfaces is far from comprehensive.

Here we report on a thermal evaporation dynamics of Au nanoparticles on single crystal oxide substrates, including MgO, $SrTiO_3$, and Al_2O_3, when varying systematically surrounding conditions. The size reduction rate of Au nanoparticles via thermal treatments was found to be strongly dependent on not only temperature but also pressure. We present a simple model to interpret the evaporation dynamics, which explains the pressure dependence on the evaporation rate of Au nanoparticles.

II. EXPERIMENT

The overall experimental procedure to tailor the size of Au particle arrays is shown schematically in Fig. 1. A polydimethylsiloxane (PDMS, Dow Corning) mold with pillar size of 650 nm (width) × 650 nm (width) × 400 nm (height) and spacing of 1000 nm was utilized to fabricate Au array patterns on single crystal oxide substrates, including MgO, $SrTiO_3$, and Al_2O_3, by the capillary force assisted contact printing technique [38–40]. First, photoresist AZ 5206-E (Hoechst) diluted by AZ 5200 thinner (Hoechst) was coated on the substrate with a thickness of about 200 nm by conventional spin coating. Immediately, the PDMS mold was carefully attached with the photoresist gel. Conformal contact between the mold and the substrate can be formed due to a strong capillary interaction. Once the molding process was completed via a soft baking at 60 °C for 3 min, the PDMS mold was allowed to detach from the substrate. A residual resist layer at the bottom of the pattern was etched by oxygen plasma (100 W, 4.0 Pa, and 35 s). Finally, Au pad patterns can be obtained by depositing 20 nm Au film and a subsequent lift-off process. Figure 2(a) shows a SEM image of the initial Au pattern with 650 nm × 650 nm and spacing of 1000 nm. By annealing at 900 °C under atmospheric pressure for 10 min, the Au pad film agglomerates to become a hemispherical-nanoparticle shape through a dewetting process [41,42], as shown in Fig. 2(b). By assuming a hemispherical shape of Au nanoparticles, the diameter of the dewetted nanoparticle volume can be estimated from the initial total nanoparticle volume [43]. As shown in Fig. 2(c), the estimated diameter from the initial Au

*To whom correspondence should be addressed: yanagi32@sanken.osaka-u.ac.jp (T.Y.); kawai@sanken.osaka-u.ac.jp (T.K.).

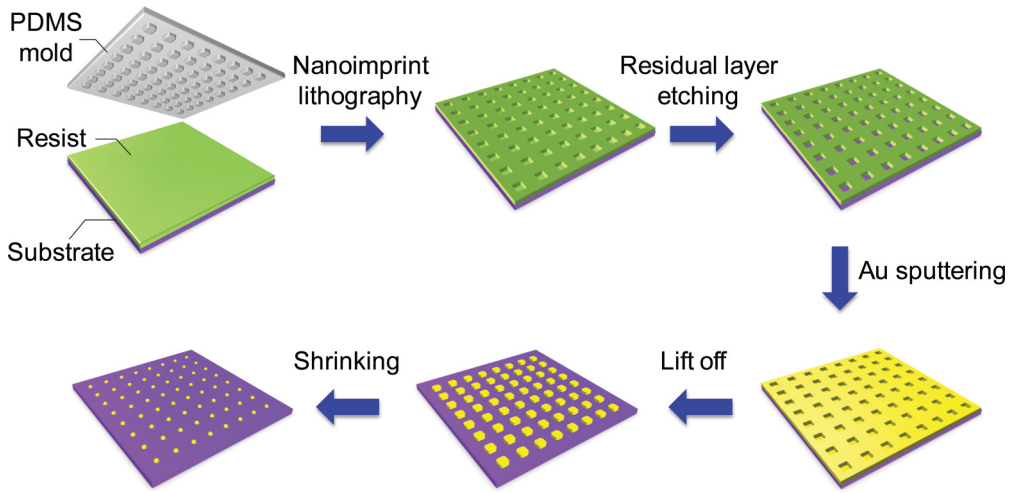

FIG. 1. (Color online) Employed process to perform a size reduction of Au nanoparticle arrays by thermal treatment. This process includes patterning submicron hole arrays by nanoimprint lithography, etching a residual resist layer by O_2 plasma, sputtering Au film, lift-off process of resist, and thermal treatment in furnace.

nanoparticle volume is consistent with the measured average diameter of nanoparticles after dewetting.

Thermal treatments were conducted in a handmade horizontal tube furnace, where a temperature and surrounding gas pressure can be controlled with relatively low background pressure of 10^{-4} Pa, which allows us to vary a surrounding pressure over a wide range. The initial Au patterned sample was placed in the center of the tube furnace. After that, high-purity Ar (99.9%) with a flow rate of 6 SCCM (SCCM denotes cubic centimeters per minute at STP) was introduced into the quartz tube, and the ambient Ar pressure was set to be

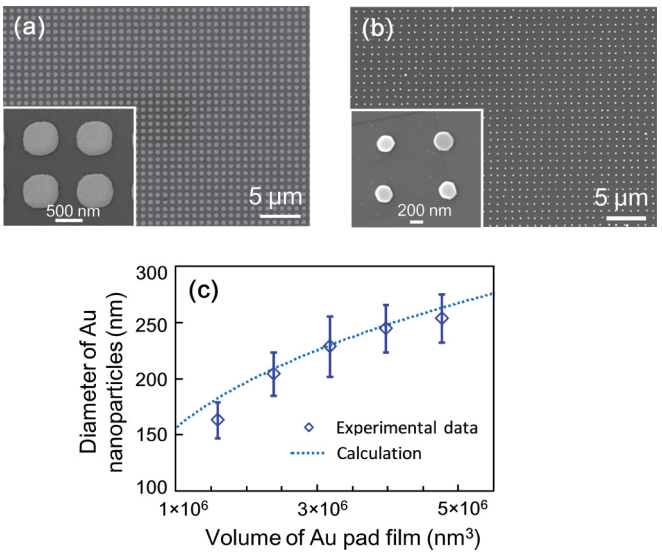

FIG. 2. (Color online) (a) SEM image of Au pad arrays patterned by nanoimprint lithography. Inset shows a magnified image. (b) SEM image of Au nanoparticle arrays with size of 290 nm after a dewetting process. (c) Correlation between a diameter of dewetted Au nanoparticles and a volume of Au pad film. Rhombus symbol represents a mean diameter of dewetted nanoparticles measured by SEM. Dashed line shows the diameter values, which are calculated by assuming a shape transformation from a slab to a hemisphere.

$10–10^5$ Pa. Then the furnace was heated up to 800 °C–950 °C with a raising rate of 15 °C/min, and kept for 5 min–20 h. Below 800 °C, no significant evaporation of Au nanoparticles was found. On the other hand, above 1000 °C a bumping rather than evaporation occurs and Au nanoparticles disappeared within several tens of minutes; the rate is too fast to measure as time series data. Thus we have performed thermal evaporation experiments for the temperature range of 800 °C–950 °C. After cooling down to room temperature, the diameter of the Au particles arrays was examined by field-emission scanning electron microscopy (FESEM) (JEOL JSM-7001F). The size measurements were performed at least for 300 nanoparticles to obtain a statistical reliability. The Au nanoparticles were also evaluated by high-resolution transmission electron microscopy (HRTEM) (JEOL JEM-3000F).

III. RESULTS AND DISCUSSIONS

Figures 3(a) and 3(b) show typical time series data of diameters of Au nanoparticles during thermal treatments. These thermal treatments were performed for Au nanoparticle arrays on MgO substrates by varying temperatures ranging from 800 °C to 950 °C, and Figs. 3(a) and 3(b) show the data under Ar pressures of 10^5 and 10 Pa, respectively. Clearly there is a significant difference between the two different Ar pressures on the trend of size reduction of Au nanoparticles. In Ar pressure of 10^5 Pa, the size reduction rate remains quite slow, even when increasing the temperature from 800 ° to 950 °C. For example, for the highest temperature, 950 °C, the size reduction rate (defined as a diameter change of Au nanoparticles per unit of time) is still 5.0 nm/h. On the other hand, for Ar pressure of 10 Pa the size reduction rate increases more drastically when increasing the temperature. For instance, at 950 °C the size reduction rate is 136 nm/h, which is in fact 27 times faster than that for 10^5 Pa. Figure 3(c) shows the mapping data of the size reduction rate of Au nanoparticles on MgO substrates when varying both temperature and Ar pressure. Here we define the size reduction rate as an averaged size reduction rate between the initial size

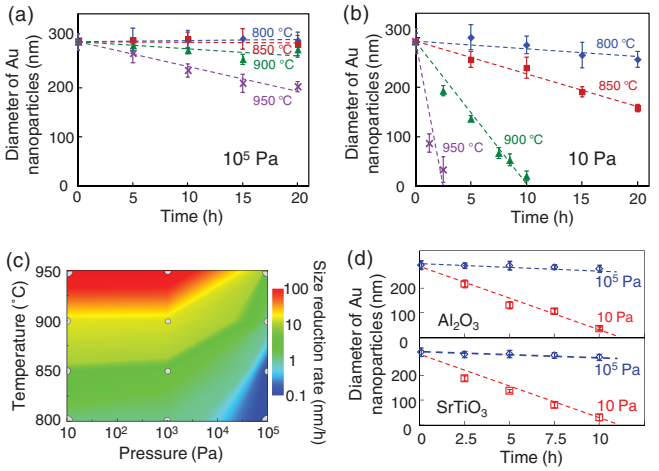

FIG. 3. (Color online) Size reduction of Au nanoparticle arrays under various temperatures under the surrounding Ar pressure of (a) 10^5 Pa, (b) 10 Pa. (c) Mapping data of size reduction rate as a function of temperature and surrounding Ar pressure. Dashed circle indicates the experimental conditions under which we have performed experiments. MgO substrate is utilized in (a)–(c). (d) Dependence of substrate materials on a size reduction of Au nanoparticles via thermal treatments. Data on Al_2O_3 and $SrTiO_3$ substrates are shown.

and the reduced size at the end of the thermal treatment for each condition. For 850 °C, the difference between 10 and 10^5 Pa on the size reduction rate is over 30 times. Clearly, lowering a pressure of inert Ar surrounding gas significantly increases the size reduction rate for the used temperature range. Thus these results highlight that surrounding pressure plays an important role in size reduction of Au nanoparticles on oxide substrates via thermal treatment. This trend as to the surrounding pressure effects has been consistently observed for other oxide substrates, including $SrTiO_3$ and Al_2O_3, as can be seen in Fig. 3(d). This insensitivity of substrate materials to the thermal evaporation events infers the minor contribution of intermixing effects between a substrate and Au nanoparticles during the evaporation events [44,45]. Figure 4 shows the cross-sectional TEM image of an interface between Au nanoparticles and $SrTiO_3$ substrate after thermal treatment of 16 h at 900 °C. The clear interface can be seen

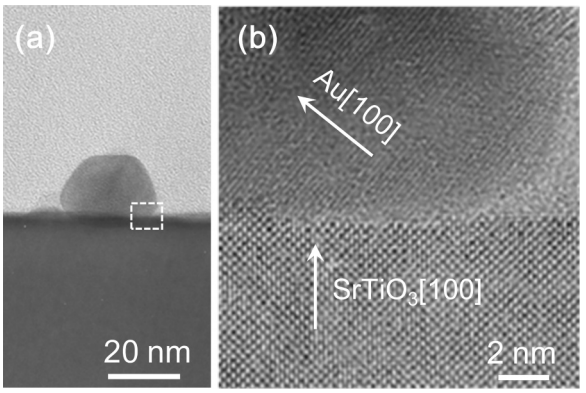

FIG. 4. (a) Typical HRTEM cross section image of Au nanoparticle on $SrTiO_3$ substrate. (b) High-magnification image of Au-$SrTiO_3$ interface.

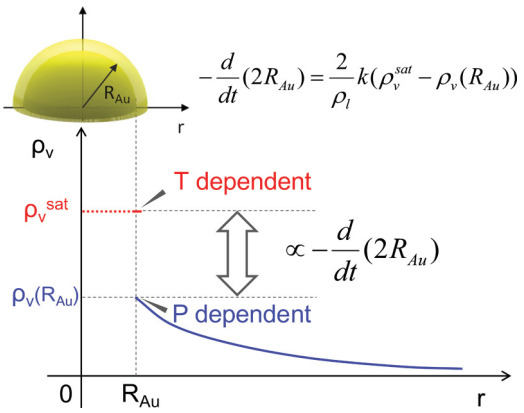

$$-\frac{d}{dt}(2R_{Au}) = \frac{2}{\rho_l}k(\rho_v^{sat} - \rho_v(R_{Au}))$$

$$\propto -\frac{d}{dt}(2R_{Au})$$

FIG. 5. (Color online) Schematic of a thermal size reduction of Au nanoparticles arrays. Spatial vapor density distribution of Au atoms $\rho_v(r)$ in a spherical coordinate system is shown. Size reduction rate of nanoparticles is determined by a vapor density difference between saturated vapor density and actual vapor density around a nanoparticle surface.

in the image, highlighting that the intermixing through the interface is negligible at least within the range of experimental conditions and materials employed [46]. In addition, the Au nanoparticles are a crystalline state because our present cooling time is quite long, more than 3 h, which might be long enough to crystallize for Au nanoparticles during cooling. These results demonstrate that a mass transport from a surface of Au nanoparticles dominates a thermal evaporation (or sublimation) of Au nanoparticles in our experiments.

Next, we discuss the observed thermal evaporation dynamics of Au nanoparticles on oxide substrates, especially the remarkable surrounding pressure effects. Consider a thermal evaporation behavior of Au hemispherical nanoparticles on oxide substrates, as illustrated in Fig. 5. In order to model a mass transport phenomenon from a surface of Au nanoparticles into the surroundings (i.e., evaporation or sublimation process), we utilize a variable r, which is defined as a distance from the center of the hemispherical Au nanoparticle. We also define a spatial density distribution of Au atoms in the gas phase as $\rho_v(r)$, when r is larger than a radius of the Au nanoparticle (R_{Au}). Here we suppose a pseudoequilibrium condition between a gas and a nanoparticle. In a thermal evaporation phenomenon, two important physical quantities, including a gas-phase density of Au at the nanoparticle surface $\rho_v(R_{\mathrm{Au}})$ and a saturated vapor density of Au (ρ_v^{sat}) must be considered to understand a thermal evaporation [47]. In addition, two major mass transfer processes coexist and dominate the thermal evaporation process. One is a mass transfer process at the surface of a nanoparticle via evaporation, and the other is a mass transfer process into the surroundings via diffusion. Considering the two major mass transfer processes, we can describe the thermal evaporation dynamics as follows.

By defining evaporation flux (j^{ev}), which is a net mass transfer rate through unit of surface to surrounding gas phase per unit of time, the temporal change of a hemispherical Au nanoparticle can be expressed as

$$\frac{d}{dt}\left(\frac{2}{3}\pi R_{\mathrm{Au}}^3 \rho_l\right) = -2\pi R_{\mathrm{Au}}^2 j^{\mathrm{ev}}, \qquad (1)$$

where ρ_l is the bulk density of an Au particle as shown in Fig. 5. Since $j^{\rm ev}$ can be empirically expressed as the product of evaporation rate constant k and density difference $[\rho_v^{\rm sat} - \rho_v(R_{\rm Au})]$ on the surface ($r = R_{\rm Au}$) of an Au particle [48],

$$j^{\rm ev} = k\left[\rho_v^{\rm sat} - \rho_v(R_{\rm Au})\right]. \tag{2}$$

Based on Eqs. (1) and (2), a size reduction rate of Au nanoparticles is described as

$$-\frac{d(2R_{\rm Au})}{dt} = \frac{2k}{\rho_l}\left[\rho_v^{\rm sat} - \rho_v\left(R_{\rm Au}\right)\right], \tag{3}$$

though, strictly speaking, a saturated vapor density $\rho_v^{\rm sat}$ depends on a radius, $R_{\rm Au}$, via a surface tension and on a total vapor pressure. However, since such dependences are very weak within our experimental range (see Appendix), $\rho_v^{\rm sat}$ can be assumed as simply the function of temperature. The evaporation rate constant k also can be assumed as a constant at a given temperature. For the semiquantitative discussion, Au spatial density distribution in the gas phase can be expressed in terms of a diffusion mechanism. The diffusion equation of a spherical coordinate system can be solved by use of static approximation and a boundary condition of $\rho = 0$ at $r = \infty$. The steady state solution is $\rho(r) = R_{\rm Au}\rho(R_{\rm Au})/r$, and flux $j^{\rm diff}$ is given by a product of diffusion constant D and divergence of ρ, i.e.,

$$j^{\rm diff}(r) = DR_{\rm Au}\rho\left(R_{\rm Au}\right)/r^2. \tag{4}$$

Using Eqs. (2)–(4) and the continuity, $j^{\rm ev} = j^{\rm diff}$, at the surface, $r = R_{\rm Au}$, we can obtain the following simplified formula:

$$\begin{aligned} -\frac{d}{dt}\left(2R_{\rm Au}\right) &= \frac{2k}{\rho_l}\rho_v^{\rm sat}\left(\frac{D/R_{\rm Au}}{D/R_{\rm Au}+k}\right) \\ &\approx \frac{2k}{\rho_l}\rho_v^{\rm sat}\left(\frac{1}{1+\alpha R_{\rm Au}P}\right), \end{aligned} \tag{5}$$

where α is a constant parameter and P is surrounding pressure. In this formula, we assume $D \propto P^{-1}$ based on Chapman-Enskog theory [49].

Two mass transfer processes such as evaporation kinetics from a surface and diffusion dynamics into the surroundings strongly govern a thermal evaporation rate of Au nanoparticles. Equation (3) describes the contributions of two such mass transfer processes as a difference between $\rho_v^{\rm sat}$ and $\rho_v(R_{\rm Au})$. When $\rho_v^{\rm sat}$ is much larger than $\rho_v(R_{\rm Au})$, a size reduction rate $-d2R_{\rm Au}/dt$ can be approximated to $k\rho_v^{\rm sat}/\rho_l$. Equation (5) indicates that such evaporation limited process can occur when pressure is low. This is a good approximation for actual experimental conditions with relatively high temperatures and fast diffusion phenomena with low surrounding pressures. On the other hand, under the high-pressure range (associated with small diffusion constant), a size reduction rate $-d2R_{\rm Au}/dt$ can be approximated to $\rho_v^{\rm sat}D/(\rho_l R_{\rm Au})$. In this case we call a diffusion limited process for constant temperature configurations [48,50]. According to Chapman-Enskog theory [49], a surrounding pressure influences a diffusion constant of atoms. Thus the idea of the diffusion controlled evaporation process is a first qualitative explanation for the surrounding pressure effect experimentally observed in Fig. 3.

Using Eqs. (3) and (5), let us consider more quantitatively a size reduction of Au nanoparticles. When Ar pressure is relatively low, that is, a diffusion process into the surroundings is fast enough, a size reduction rate should be approximated to $\rho_v^{\rm sat}/\rho_l$, as previously discussed. Figure 6 shows the temperature dependence of a size reduction rate of Au nanoparticles. The thermal treatments were performed for Au nanoparticle arrays on MgO substrate under constant Ar pressure of 10 Pa. In the figure, we estimated a saturated vapor density of Au when varying a temperature, and such estimated data were plotted. Saturated vapor density $\rho_v^{\rm sat}$ as a function of temperature was estimated using the Antoine equation and the ideal gas law equation as

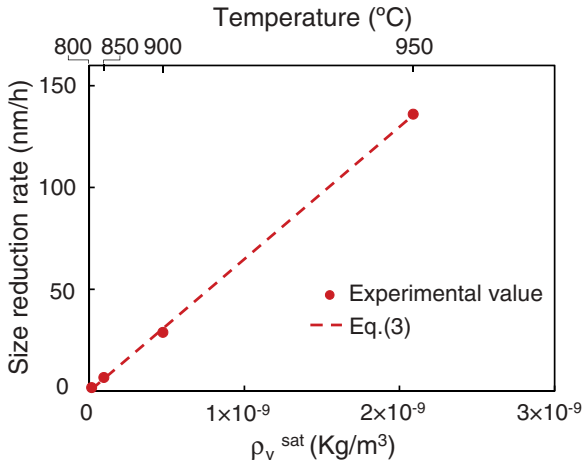

FIG. 6. (Color online) Temperature dependence of a size reduction rate of Au nanoparticles. Surrounding Ar pressure is 10 Pa, and MgO substrate is used. The dashed line shows $-d2R_{\rm Au}/dt = k\rho_v^{\rm sat}/\rho_l$, with a constant k.

$$\rho_v^{\rm sat} = \frac{M}{RT}10^{A-\frac{B}{T}-C\ln T}, \tag{6}$$

where R is a gas constant; $R = 8.314\,{\rm J\,K^{-1}\cdot mol^{-1}}$; M is molar mass of Au; $M = 197$ g/mol; A, B, and C are component-specific constants; $A = 14.158$, $B = 19\,343$, and $C = 0.7479$ [51]. The linear relationship between a size reduction rate $-d2R_{\rm Au}/dt$ and a saturated vapor pressure $\rho_v^{\rm sat}$ can be seen. Clearly our temperature dependence data are a good fit to the proposed Eq. (3).

Next we analyze the surrounding pressure effect. According to Eq. (5), the average size reduction rate is described as

$$\overline{dR_{\rm Au}/dt} \equiv R_{\rm Au}^{\rm ini}/\tau = \frac{k}{\rho_l}\rho_v^{\rm sat}\left(\frac{1}{1+\alpha R_{\rm Au}^{\rm ini}P/2}\right), \tag{7}$$

where τ is the time scale for an Au nanoparticle with initial radius $R_{\rm Au}^{\rm ini}$ to vanish. Figure 7 shows a size reduction rate of Au nanoparticles under various surrounding Ar pressures ranging from 10^5 to 10 Pa. The thermal treatments were performed for Au nanoparticle arrays on MgO substrate under a constant temperature of 900 °C. Increasing the surrounding pressure decreases the size reduction rate, especially around 10^3–10^4 Pa range. As clearly seen in Fig. 7, Eq. (7) can well describe experimental data. Namely, the faster size reduction at lower pressures must be due to the faster diffusion in the gas phase, while thermal evaporation under higher pressures is greatly limited by smaller diffusion rate in the gas phase. The agreement gives a semiquantitative interpretation

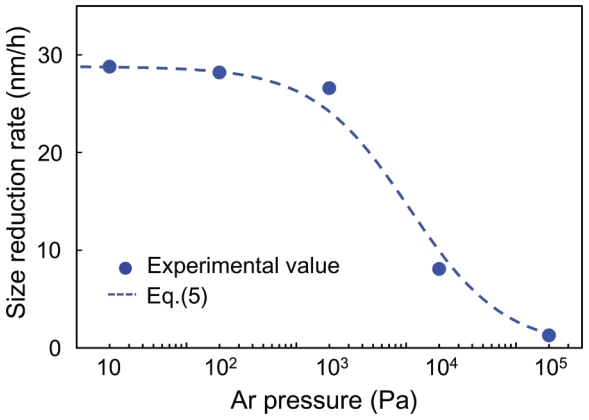

FIG. 7. (Color online) Pressure dependence of a size reduction rate of Au nanoparticles. Temperature is 900 °C, and MgO substrate is used. The dashed curve is the model line using Eq. (7).

of how diffusion processes in a gas phase affect the size reduction of Au nanoparticles. Thus we conclude that Eqs. (5) and (7) can give a semiquantitative description as to the surrounding pressure effects on the thermal size reduction of Au nanoparticles.

Based on the above knowledge as to the significant surrounding pressure effect on a thermal size reduction, one can expect that manipulating a surrounding pressure gives an effective approach to control precisely a size reduction rate of noble metal nanoparticles. This is because pressure is in general the easiest controlling parameter with more rapid stabilization than other parameters including temperature. Although a heating system for large samples usually needs quite a long time to stabilize a temperature when changing the temperature, a pressure can be immediately altered and stabilized within a few seconds even in the larger heating system as long as the chamber is well designed for pumping. As one example for the pressure-control capability, we performed two-step size reduction experiments at a constant temperature of 900 °C. At the first step, the lower Ar pressure of 10 Pa was applied for 6 h to reduce the nanoparticles array for a relatively short time, and after that the pressure was rapidly increased to 1×10^4 Pa in order to achieve a slower size reduction rate with diffusion-limited mode. The observed behavior is shown in Fig. 8. Variation of shrinking rate depending on the pressure is clearly observed in Fig. 8(a), and the size reduction rates were 28.8 nm/h or 10.0 nm/h for each step. Figure 8(b) shows SEM images of reduced Au nanoparticles during the two-step size reduction process. Size of Au nanoparticles can be gradually varied from 290 nm to ~10 nm. In each stage, Au nanoparticle arrays have nearly identical size, demonstrating no inhomogeneous mass exchange among particles, like Ostwald ripening or other effects [52,53]. This might be due to relatively large distance between particles in this study, and the effect of the interaction between neighboring diffusion fields would be an interesting issue by altering the initial distance between particles on the substrate. The smallest Au nanoparticles arrays by two-step shrinking is about 10 nm. Here it is noted that this is not the intrinsic limitation of thermal size reduction process, and obviously further size reduction down to several nanometers should be possible. A

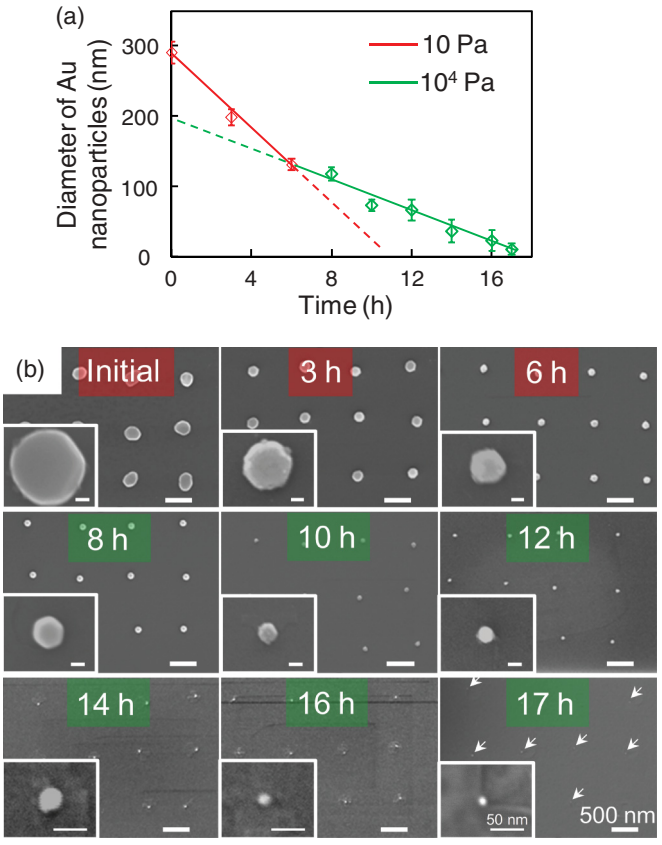

FIG. 8. (Color online) Application of pressure-induced evaporation dynamics to precisely control and tailor the size of Au nanoparticles. (a) Pressure alternation effect on a size reduction rate control. A fast (28 nm/h) size reduction rate is utilized for submicron scale, and when Au nanoparticles size is reduced around 100 nm, we increase the surrounding pressure to reduce a size reduction rate via switching into a diffusion limited mode (with moderate shrinking rate of 10 nm/h) (b) SEM images as to a temporal change of thermal evaporation of Au nanoparticles during the two-step evaporation process.

pressure-controllable heating system is very simple apparatus; thus the combination of standard lithography and thermal shrinking with pressure control offers one of the simplest but powerful methods to create sublithographic scale nanoparticle arrays with desired spatial locations for large scale.

IV. CONCLUSION

We have demonstrated that a size reduction rate of gold nanoparticles via evaporation is strongly dependent on not only temperature but also pressure. Lowering pressure enhances the evaporation rate of gold nanoparticles over 30 times at the same temperature. The temperature dependence is solely due to the variation of the saturated vapor pressure of gold under the low-pressure inert gas condition, whereas the pressure dependence of the surrounding inert gas on the evaporation of gold nanoparticles can be interpreted in terms of a pressure dependence on the gas-phase diffusion of evaporated gold species. We present a model to explain the evaporation dynamics, which well describes quantitatively the pressure dependence on evaporation of gold nanoparticles in terms

of a variation of vapor pressure value around a liquid-vapor interface. By utilizing a facile evaporation technique based on the above principles, we succeeded in controlling precisely a size reduction of Au nanoparticle down to −10 nm diameter range from −300 nm initial size.

ACKNOWLEDGMENTS

This study was in part supported by a Grant-in-Aid for Scientific Research on Innovative Areas [20111004] from the Ministry of Education, Culture, Sports, Science and Technology (MEXT) of Japan. F.Z., B.X., G.M., and Y.H. were supported by NEXT. T.K. was supported by the FIRST program.

APPENDIX

Suppose that a pure Au system is in vapor-liquid coexistence at its chemical potential μ_o and pressure P_0. Considering a pressure equilibrium between total vapor pressure $P^{\rm tot}$ and that of Au liquid under the existence of an inert gas, the shift of Au equilibrium chemical potential $\Delta\mu$ satisfies $\Delta\mu < P^{\rm tot}/\rho l$, using the Gibbs-Duhem equation $d\mu/dP = 1/\rho$ under the constant temperature. Thus the saturated vapor pressure of Au, $P_v^{\rm sat}$, also differs from P_0 and the difference ΔP satisfies

$$\frac{\Delta P}{P_0} < \frac{\rho_v^0 P^{\rm tot}}{\rho_l P_0} \approx \frac{P^{\rm tot}}{\rho_l k_B T/M}, \tag{A1}$$

with the saturated vapor pressure in a pure Au system ρ_v^0. In our experimental condition $P^{\rm tot}$ is not higher than 10^5 Pa; the saturated density dependence on the inert gas pressure is almost negligible.

For a spherical nanoparticle of Au liquid, the saturated vapor density also depends on the radius via the surface tension at the vapor-liquid interface as

$$\rho_v^{\rm sat}(R) \approx \rho_v^0 + \frac{M}{k_B T}\frac{2\gamma}{R}. \tag{A2}$$

In the range where the last term in Eq. (A2) is dominant, the evaporation rate would sensitively depend on the radius. The linear profile of the size reduction rate is shown in Fig. 3 as the long time behavior suggests that the surface effect is relatively weak in our observation range.

[1] C. T. Campbell and C. H. F. Peden, Science **309**, 713 (2005).
[2] J. N. Anker, W. P. Hall, O. Lyandres, N. C. Shah, J. Zhao, and R. P. Van Duyne, Nat. Mater. **7**, 442 (2008).
[3] A. N. Shipway, E. Katz, and I. Willner, Chem. Phys. Chem. **1**, 18 (2000).
[4] K. Nagashima, T. Yanagida, H. Tanaka, and T. Kawai, J. Appl. Phys. **101**, 124304 (2007).
[5] K. Nagashima, T. Yanagida, H. Tanaka, and T. Kawai, Appl. Phys. Lett. **90**, 233103 (2007).
[6] A. Marcu, T. Yanagida, K. Nagashima, H. Tanaka, and T. Kawai, J. Appl. Phys. **102**, 016102 (2007).
[7] T. Yanagida, K. Nagashima, H. Tanaka, and T. Kawai, Appl. Phys. Lett. **91**, 061502 (2007).
[8] K. Nagashima, T. Yanagida, H. Tanaka, S. Seki, A. Saeki, S. Tagawa, and T. Kawai, J. Am. Chem. Soc. **130**, 5378 (2008).
[9] A. Marcu, T. Yanagida, K. Nagashima, K. Oka, H. Tanaka, and T. Kawai, Appl. Phys. Lett. **92**, 173119 (2008).
[10] T. Yanagida, K. Nagashima, H. Tanaka, and T. Kawai, J. Appl. Phys. **104**, 016101 (2008).
[11] K. Nagashima, T. Yanagida, K. Oka, H. Tanaka, and T. Kawai, Appl. Phys. Lett. **93**, 153103 (2008).
[12] T. Yanagida, A. Marcu, H. Matsui, K. Nagashima, K. Oka, K. Yokota, M. Taniguchi, and T. Kawai, J. Phys. Chem. C **112**, 18923 (2008).
[13] K. Oka, T. Yanagida, K. Nagashima, H. Tanaka, and T. Kawai, J. Am. Chem. Soc. **131**, 3434 (2009).
[14] A. Klamchuen, T. Yanagida, K. Nagashima, S. Seki, K. Oka, M. Taniguchi, and T. Kawai, Appl. Phys. Lett. **95**, 053105 (2009).
[15] K. Oka, T. Yanagida, K. Nagashima, H. Tanaka, S. Seki, Y. Honsho, M. Ishimaru, A. Hirata, and T. Kawai, Appl. Phys. Lett. **95**, 133110 (2009).
[16] K. Nagashima, T. Yanagida, A. Klamchuen, M. Kanai, K. Oka, S. Seki, and T. Kawai, Appl. Phys. Lett. **96**, 073110 (2010).
[17] K. Nagashima, T. Yanagida, K. Oka, M. Taniguchi, T. Kawai, J. S. Kim, and B. H. Park, Nano Lett. **10**, 1359 (2010).
[18] K. Oka, T. Yanagida, K. Nagashima, T. Kawai, J. S. Kim, and B. H. Park, J. Am. Chem. Soc. **132**, 6634 (2010).
[19] M. Suzuki, Y. Hidaka, T. Yanagida, M. Kanai, T. Kawai, and S. Kai, Phys. Rev. E **82**, 011605 (2010).
[20] A. Klamchuen, T. Yanagida, M. Kanai, K. Nagashima, K. Oka, T. Kawai, M. Suzuki, Y. Hidaka, and S. Kai, Appl. Phys. Lett. **97**, 073114 (2010).
[21] A. Klamchuen, T. Yanagida, M. Kanai, K. Nagashima, K. Oka, T. Kawai, M. Suzuki, Y. Hidaka, and S. Kai, J. Cryst. Growth **312**, 3251 (2010).
[22] A. Klamchuen, T. Yanagida, K. Nagashima, M. Kanai, K. Oka, S. Seki, M. Suzuki, Y. Hidaka, S. Kai, and T. Kawai, Appl. Phys. Lett. **98**, 053107 (2011).
[23] K. Nagashima, T. Yanagida, K. Oka, M. Kanai, A. Klamchuen, J. S. Kim, B. H. Park, and T. Kawai, Nano Lett. **11**, 2114 (2011).
[24] M. Suzuki, Y. Hidaka, T. Yanagida, A. Klamchuen, M. Kanai, T. Kawai, and S. Kai, Phys. Rev. E **83**, 061606 (2011).
[25] A. Klamchuen, T. Yanagida, M. Kanai, K. Nagashima, K. Oka, S. Rahong, G. Meng, M. Horprathum, M. Suzuki, Y. Hidaka, S. Kai, and T. Kawai, Appl. Phys. Lett. **99**, 193105 (2011).
[26] G. Meng, T. Yanagida, K. Nagashima, T. Yanagishita, K. Oka, M. Kanai, A. Klamchuen, S. Rahong, M. Horprathum, B. Xu, F. Zhuge, Y. He, H. Masuda, and T. Kawai, RSC Adv. **2**, 10618 (2012).
[27] F. Zhuge, T. Yanagida, K. Nagashima, M. Kanai, H. Yoshida, A. Klamchuen, M. Gang, B. Xu, Y. He, S. Rahong, X. Li, M. Suzuki, S. Kai, S. Takeda, and T. Kawai, J. Phys. Chem. C **116**, 24367 (2012).

[28] R. Grisel, K. J. Weststrate, A. Gluhoi, and B. E. Nieuwenhuys, Gold Bull. **35**, 39 (2002).
[29] M. T. Borgstrom, G. Immink, B. Ketelaars, R. Algra, and E. P. A. M. Bakkers, Nat. Nanotechnol. **2**, 541 (2007).
[30] W. Jiang, B. Y. S. Kim, J. T. Rutka, and W. C. W. Chan, Nat. Nanotechnol. **3**, 145 (2008).
[31] S. H. Lee, G. Jo, W. Park, S. Lee, Y. S. Kim, B. K. Cho, T. Lee, and W. B. Kim, ACS Nano **4**, 1829 (2010).
[32] J. Abramson, M. Palma, S. J. Wind, and J. Hone, Adv. Mater. **24**, 2207 (2012).
[33] A. Javey and H. J. Dai, J. Am. Chem. Soc. **127**, 11942 (2005).
[34] B. D. Gates, Q. B. Xu, M. Stewart, D. Ryan, C. G. Willson, and G. M. Whitesides, Chem. Rev. **105**, 1171 (2005).
[35] C. Vieu, F. Carcenac, A. Pepin, Y. Chen, M. Mejias, A. Lebib, L. Manin-Ferlazzo, L. Couraud, and H. Launois, Appl. Surf. Sci. **164**, 111 (2000).
[36] H. Ago, T. Ayagaki, Y. Ogawa, and M. Tsuji, J. Phys. Chem. C **115**, 13247 (2011).
[37] W. K. Choi, T. H. Liew, H. G. Chew, F. Zhang, C. V. Thompson, Y. Wang, M. H. Hong, X. D. Wang, L. Li, and J. Yun, Small **4**, 330 (2008).
[38] Y. N. Xia and G. M. Whitesides, Annu. Rev. Mater. Sci. **28**, 153 (1998).
[39] N. Koo, M. Bender, U. Plachetka, A. Fuchs, T. Wahlbrink, J. Bolten, and H. Kurz, Microelectron Eng. **84**, 904 (2007).
[40] N. Koo, U. Plachetka, M. Otto, J. Bolten, J. H. Jeong, E. S. Lee, and H. Kurz, Nanotechnology **19**, 225304 (2008).
[41] D. Kim, A. L. Giermann, and C. V. Thompson, Appl. Phys. Lett. **95**, 251903 (2009).
[42] C. M. Muller, F. C. F. Mornaghini, and R. Spolenak, Nanotechnology **19**, 485306 (2008).
[43] S. K. Yang, F. Xu, S. Ostendorp, G. Wilde, H. Zhao, and Y. Lei, Adv. Funct. Mater. **21**, 2446 (2011).
[44] A. Sundar, R. A. Hughes, P. Farzinpour, K. D. Gilroy, G. A. Devenyi, J. S. Preston, and S. Neretina, Appl. Phys. Lett. **100**, 013111 (2012).
[45] O. Malyi and E. Rabkin, Acta Mater. **60**, 261 (2012).
[46] C. M. Wang, V. Shutthanandan, Y. Zhang, L. E. Thomas, D. R. Baer, S. Thevuthasan, and G. Duscher, J. Appl. Phys. **95**, 5060 (2004).
[47] F. J. Harvey, Metall. Trans. **3**, 2973 (1972).
[48] E. Sultan, A. Boudaoud, and M. Ben Amar, J. Fluid Mech. **543**, 183 (2005).
[49] E. L. Cussler, *Diffusion: Mass Transfer in Fluid Systems* (Cambridge University Press, Cambridge, 1997).
[50] I. Langmuir, Phys. Rev. **2**, 329 (1913).
[51] D. R. Lide, *CRC Handbook of Chemistry and Physics* (CRC Press, Boca Raton, FL, 2003).
[52] S. Sakurai, H. Nishino, D. N. Futaba, S. Yasuda, T. Yamada, A. Maigne, Y. Matsuo, E. Nakamura, M. Yumura, and K. Hata, J. Am. Chem. Soc. **134**, 2148 (2012).
[53] P. Beruna, D. Crespo, R. Gonzalez-Cinca, and E. Pineda, J. Appl. Phys. **100**, 054907 (2006).